CONTRIBUTIONS TO THE SIZE REDUCTION OF A BATTERY USED FOR PV POWER RAMP RATE CONTROL

Aitor Makibar, Luis Narvarte, Eduardo Lorenzo

Instituto de Energía Solar, ETSIS Telecomunicación, Polytechnic University of Madrid, 28031Madrid, Spain

Abstract

In order to mitigate PV power fluctuations, ramp rate control is performed coupling battery energy storage systems to PV plants. In previous works, we analysed the effects of reducing the size of a battery designed to absorb every fluctuation by taking into consideration, both, the fluctuation occurrence and the penalties in case of non-compliance of a given prescribed ramp-rate limitation. In this work, two new techniques are proposed for enhancing the battery size reduction potential. In the first technique, part of the fluctuations is absorbed by limiting PV inverters during upwards fluctuations. A new control strategy has been created to team up inverters limitation with a reduced battery in order to improve the ramp rate compliance of the plant. In the second technique, PV array oversizing is studied as an alternative to mitigate part of the fluctuations. The results show that for the same storage size, a proper combination of these solutions increases the yearly PV production under the conditions of a specific grid-code, creating new tools for selecting a battery with reduced power and energy capacity.

1. Introduction

During the next years, a large share of photovoltaic (PV) power is expected to be integrated in worldwide electricity grids, but, in order to achieve it, grid-stability and power quality problems must be avoided (EPIA, 2012). In certain regions with low interconnected and/or weak grids such as islands, installing utility-scale PV plants implies increasing considerably their share in the electricity mix. In this scenario, short-term PV power fluctuations caused by clouds are raising the attention of TSOs of such grids, because they represent troubles for maintaining the frequency and voltage stability (Marcos et al., 2011a). They have started to propose strict grid codes aiming to reduce the power fluctuations, imposing ramp rate (RR) limitations to individual plants. One of the most relevant code was proposed by the Puerto Rico Electric Power Authority (PREPA, 2012), by imposing a RR limitation which restricts the output variation to 10% of the PV plant nameplate power per minute, RR_{LIM} = 10%/min. Other TSOs are also concerned about this matter (CRE, 2012; HECO, 2014; NERC, 2012).

Under this scenario, several procedures have been proposed to characterise PV power fluctuations and to develop techniques to mitigate them. The most classical references had a lack of measurements, so artificial data series were created for simulating intermittent irradiance conditions (Chowdhury, 1992; Chowdhury and Rahman, 1987). Later, measured data was used to characterise irradiance fluctuations in the domain of frequency. (Otani et al., 1997) addressed their spectral density by correlating data measured at nine stations, giving importance to the area of incidence. In (Woyte et al., 2007a, 2007b, 2006) pseudorandom time series of irradiance dataset was used, obtained with measured data of clearness index and treated as realizations of a stochastic, locally stationary, wavelet process. (Tomson and Tamm, 2006) also modelled them as exponential distribution functions.

Currently PV power fluctuations are characterised directly, depending, among others, on the size of the PV plant and the speed of the clouds that cover the arrays (Hoff and Perez, 2010; Lave and Kleissl, 2013; Mazumdar et al., 2014; Mills et al., 2009; Van Haaren et al., 2014). In (Marcos et al., 2011a) fluctuations are characterised in the domain of the frequency and studying their probability of occurrence along a given year. The frequency distribution is empirically modelled as an exponential decay function and it demonstrates that the occurrence of medium-to-strong size fluctuations in a utility-scale PV plant is very

low. Besides, the authors propose a model that predicts the output power of a PV plant using data of incident irradiance (Marcos et al., 2011b).

PV power fluctuations can be smoothed by taking into account their nature and the influence of design parameters of a PV plant. As the area of the PV array increases, both the maximum power fluctuation registered and the 90^{th} percentile of every fluctuations are reduced exponentially (Marcos et al., 2011a). Fluctuations can also be smoothed by geographically dispersing PV plants. When several plants are separated but still located inside the same region to aggregate their power, the probability that a cloud front covers all of them simultaneously is highly reduced and each plant compensates the fluctuations occurred in another plant separated by sufficient distance. In (Murata et al., 2009; Murata and Otani, 1997), simulated and measured PV power data are used for analysing the effect of distributing a large number of PV plants along a country-level region; obtaining a correlation between power fluctuations and the distances between plants. A similar work was done in (Hoff and Perez, 2010; Lave et al., 2012; Marcos et al., 2012; Mills et al., 2009). For a certain aggregated power, fluctuations are smoothed as the number of dispersed PV plants increases.

However, in some regions like islands, the potential for dispersing plants is intrinsically limited (Lave et al., 2012; Marcos et al., 2012), so the strict grid regulations of these regions demand buffering capabilities to individual PV plants. This concept is known as ramp rate control and requires a battery energy storage system (BESS). By analysing PV power fluctuations statistically, in (Perez and Hoff, 2013; van Haaren et al., 2015) this issue is addressed. In line with this and based on one second long-term observations at PV plants of different sizes, a model for the "worst fluctuation" (WF) was proposed in (Marcos et al., 2014b). Roughly, it corresponds to the fastest darkening of the PV array (from clear sky irradiance to diffuse irradiance) by a cloud moving at about 80-90 km/h, pace which is also confirmed by (Lave and Kleissl, 2013). Providing the battery can be fully recharged between consecutive fluctuations by means of a state of charge (SOC) driven control, the WF model allows sizing the battery for full compliance of ramp-rate limits (Marcos et al., 2014a, 2014b). As a next step, more recent studies are focused on reducing the storage requirements. Thus, several control strategies have been developed in order to optimise the usage of batteries, combining their operation with other techniques (Bullich-Massagué et al., 2017; de la Parra et al., 2016, 2015; Ina et al., 2004; Sukumar et al., 2018; van Haaren et al., 2015).

In this context, in (Makibar et al., 2017) a method for evaluating the potential for reducing the battery size was developed. The study is based on the fact that strong fluctuations scarcely occur, so it assesses the impact of reducing the size of a battery initially designed to absorb every fluctuation, by taking into consideration, both, the fluctuation occurrence and the penalties applied in case of non-compliance with the RR limitation. That work demonstrated that it is possible to reduce the battery size up to 30% of the nominal values without incurring in penalties. In the present paper, two new techniques are going to be studied to reduce storage requirements below that limit.

2. Methodology

The research methodology followed in this work is based on the process described in (Makibar et al., 2017). Same experimental database is used but, in this case, two new techniques are implemented in the battery size reduction assessment. On the following, first, the experimental data used for the analysis and the size reduction assessment method of (Makibar et al., 2017) are briefly explained as reminder and, second, the two novel techniques are presented with the aim of upgrading the method. Finally, different comparative studies are carried out to assess their potential, presenting the results in the next section

2.1 Experimental data

Extensive simulation exercises were performed using as input one second power values recorded at the point of common coupling of a 7.2 MW PV plant located in Milagro, northern Spain. This plant is equipped with vertical axis trackers covering an area of 52 ha. Besides, other relevant parameters such as

horizontal and tilted irradiance were measured by calibrated modules. PV power data series is used for analysing the behaviour of the plant under study against the control strategy developed in the first technique. Irradiance data is useful to develop the second technique, which needs to simulate the output power of a PV plant whose design parameters are modified with respect to the original Milagro PV plant.

2.2 Battery size reduction assessment

The study uses as showcase the regulation proposal of Puerto Rico (PREPA, 2012). It requires the use of a battery to match the prescribed RR limit of 10%/min and it considers penalties through PV power curtailment for complete week periods, as a function of RR non-compliance observed the week before. In this context, optimal battery size from the viewpoint of the PV plant owner results from a trade-off between battery investment costs and applicable penalties in case of non-compliance with RR limitation.

The starting point of the method is a full-size battery designed to absorb 100% of fluctuations that could be observed at the output of a PV plant, sized according to the WF model and operated by a basic SOC control algorithm. In order to allow Milagro PV plant for complying with RR_{LIM} = 10%/min, the battery power and energy requirements are respectively $P_{\mathrm{BAT,WF}} = 5148\mathrm{kW}$ and $C_{\mathrm{BAT,WF}} = 437\mathrm{kWh}$. Given that the sign of the first fluctuation is unknown, the energy requirement must be doubled to absorb both downwards and upwards fluctuations, so the full-size battery has a power and capacity of $P_{\mathrm{BAT,WF}} = 5148\ \mathrm{kW}\ \ (71\%\ P_{\mathrm{N}})$ and $2 \cdot C_{\mathrm{BAT,WF}} = 874\ \mathrm{kWh}\ \ (7.2\ \mathrm{min})$ respectively. Hence, the basic algorithm restores the battery to *SOC* = 50% before the start of every new fluctuation, so we can name it as *SOC50* strategy.

The practical implementation procedure of the battery size reduction assessment method, consists on the following.

The PV power injected to the grid, P_{GRID}, is scanned every 2 seconds and by measuring the *RR* between every scan, their compliance with the RR_{LIM} is evaluated. Reducing the battery power and/or capacity by a certain factor, named respectively as k_p and k_c, will prevent the battery from absorbing some fluctuations, lowering the compliance of the scans involved in them.

Then, weekly RR compliance index, RRC_{w}, is calculated as a percentage of compliant scans among total scans of week w. The minimum compliance to avoid penalties is $RRC_{\mathrm{min}} = 98.5\%$, so if less percentage of scans comply with RR_{LIM}, a PV power curtailment factor is imposed for the next week, Cu_w. This penalty is cumulative and it depends on the difference between RRC of previous week and RRC_{min}.

Finally, yearly PV energy production for a reduced size battery, $E_{\mathrm{GRID},k_p,k_c}$, is calculated to evaluate the effect of reducing battery power and/or capacity. It is useful for selecting a proper combination of k_p and k_c, delimiting PV production losses derived from the penalties. It is obtained performing yearly simulations of the operation of the plant in several iterative rounds, one for each k_p and k_c combination and assessing weekly RRC and curtailments along the full year.

2.3 Reduction of storage requirements by means of a control strategy

The first technique proposed addresses PV+BESS plant control issues. In order to avoid doubling the reference battery capacity, upwards fluctuations can be absorbed by limiting the output PV power variations at each inverter locally, by moving their operation point out of the MPP. Therefore, the BESS will be used for supplying the lack of power and energy caused by downwards fluctuations uniquely, requiring half of energy capacity compared to *SOC50* strategy. Hence, full-size battery parameters are $P_{\mathrm{BAT,WF}} = 5148\ \mathrm{kW}\ (71\%\ P_{\mathrm{N}})$ and $C_{\mathrm{BAT,WF}} = 437\ \mathrm{kWh}\ (3.6\ \mathrm{min})$. Nevertheless, when PV inverters are curtailed, not all of the available PV energy is fed into the grid, so this practice involves some energy losses that must be taken into account.

The control loop implemented in this new strategy is aimed to restore the battery SOC after each downwards fluctuation is over, keeping it fully charged and ready for the next cloud that will cover the PV array. This type of strategies have been widely studied in (de la Parra et al., 2016, 2015) among others. However, in order to reduce the losses associated with inverters power limitation, some of them need additional inputs to model the PV power under clear sky conditions at any time step, like Linke turbidity factor and the measured cell temperature. For the particular purpose of our battery size reduction assessment, a new control strategy has been developed, named as *SOC100_PVCurt*, which fulfils the accuracy requirements in a simple way. It mitigates every fluctuation and it minimises the energy loss associated with inverters limitations without the need for additional inputs.

2.3.1 SOC100_PVCurt control strategy

The general idea is to use part of the excess PV power of the upwards fluctuation for recovering battery SOC to the reference value of *SOC* = 100%, instead of curtailing inverters power directly. While SOC is below the reference, all the excess PV power is used for charging the battery. Once the charge process is complete, the algorithm will send a curtailment signal to the PV inverters to smooth the rest of the upwards fluctuation event. The control diagram of *SOC100_PVCurt* strategy is shown in Figure 1.

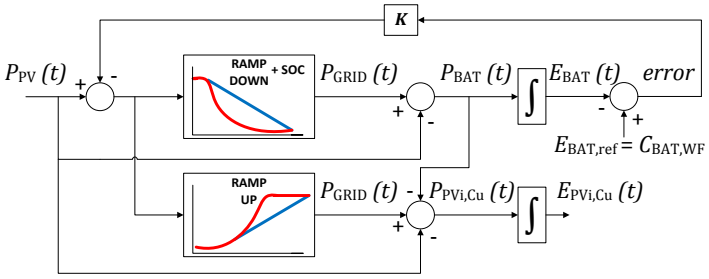

Figure 1: *SOC100_PVCurt* control diagram. Upwards fluctuations are absorbed by limiting PV inverters if battery is charged (when $E_{BAT}(t) = E_{BAT,ref}$). Downwards fluctuations are absorbed by discharging the battery.

In order to both, keep a good balance between speed and system stability and to avoid too high battery power requirements in a SOC recovery process, the value of the proportional parameter is $K = 15$. $P_{PV}(t)$ is the output of the PV plant, which is limited by RR_{LIM} to the power allowed to feed into the grid, $P_{GRID}(t)$. $P_{BAT}(t)$ is the power discharged from/charged into the battery to match the ramp, $E_{BAT}(t)$ is the energy stored in the battery at a given time and $E_{BAT,ref}$ is its reference value, corresponding to full charge and equalling the value of $C_{BAT,WF}$. Eq. (1) allows calculating PV inverters power limitation, $P_{PVi,Cu}(t)$, depending on the allowable ramp and on the power required by the battery. $E_{PVi,Cu}(t)$ is the associated loss.

$$P_{PVi,Cu}(t) = P_{GRID}(t) - P_{PV}(t) - P_{BAT}(t) \quad (1)$$

The strategy has five main operation modes. On the following, each mode is explained and illustrated by means of two simulations of Milagro PV plant operated under *SOC100_PVCurt* strategy throughout two different time lapses. The simulation of Figure 2a runs a full-size battery ($P_{BAT} = P_{BAT,WF}$ and $C_{BAT} = C_{BAT,WF}$) and explains four of the modes (a-d). The simulation of Figure 2b explains a particular mode (e) which optimises the operation of reduced batteries. In this case, it is reduced by $k_p = 0.3$, resulting a limited battery power of $P_{BAT} = k_p \cdot P_{BAT,WF} = \pm 1545$ kW.

a) *Ramp-Down* mode:

Battery supports lack of PV power to match RR_{LIM} of $P_{GRID}(t)$. (12:21- 12:25).

b) *SOC recovery / No ramp* mode:

Battery SOC is restored using part of PV power, in absence of fluctuation. (12:25-12:30).

c) *SOC recovery / Ramp-Up* mode:

Battery SOC is restored by absorbing excess PV power to match RR_{LIM}. (12:30).

d) *Ramp-Up* mode:

If battery *SOC* = 100%, PV inverters power is limited (12:53). If *SOC* < 100%, the strategy faces the first part of the fluctuation using excess PV power to charge the battery to $E_{\mathrm{BAT,ref}}$ (12:57-12:59) and then, it enters in inverters curtailment mode, doing the transition without affecting the system stability and keeping RR_{LIM}. As a result, part of $E_{\mathrm{PVi,Cu}}$ losses is saved.

e) *Limited Ramp-Up* mode:

When the battery size is reduced by k_p, the upwards ramp is matched teaming up the battery with inverters power limitation. In strong downwards fluctuations, the limited power of the battery (P_{BAT}) makes to fail the RR_{LIM} (t = 7 to t = 9), but upwards fluctuations can be fully absorbed in three steps: While excess PV power is lower than P_{BAT}, battery is charged (t = 10 to t = 13). If it is higher, inverters limitation gives support to the battery (t = 13 to t = 15). When the battery is at full-charge, the rest of the ramp is matched by limiting the inverters power (t = 15 to t=18). This way, every non-compliance that could occur during upwards fluctuations is avoided and, even with a reduced battery, the $E_{\mathrm{PVi,Cu}}$ losses are reduced.

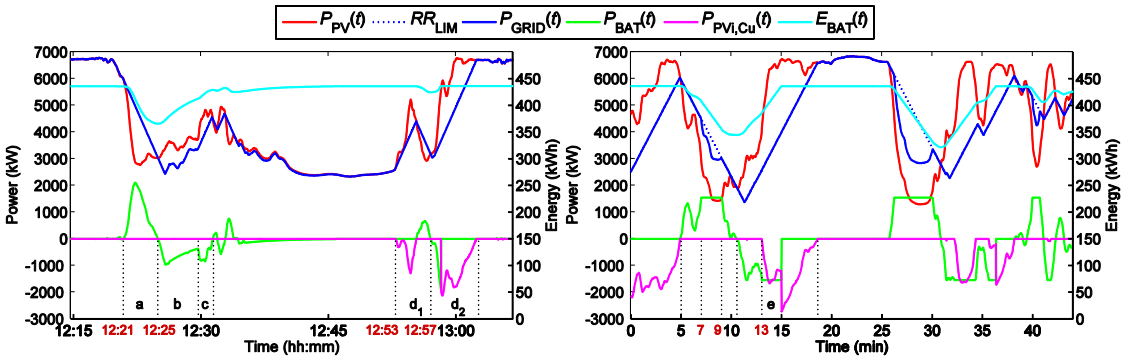

Figure 2: *SOC100_PVCurt* control strategy in operation. (a) A full-size battery rated $C_{\mathrm{BAT}} = 437$ kWh is discharged during downwards fluctuation and then, it is recharged. If battery is fully charged, PV inverter curtailment is activated. Inside an upwards fluctuation, SOC recovery / PV curtailment functions can be alternated if *SOC* = 100% is achieved. (b) If the required power for smoothing a downwards ramp is higher than the reduced battery power ($\pm$1545 kW), the fluctuation cannot be fully mitigated and the ramp is not fulfilled. In upwards ramps, power absorbed by the reduced battery is complemented by limiting inverters power, so the ramp is fulfilled.

2.3.2 Methodology to reduce battery requirements

The steps to carry out the battery size reduction assessment are the ones described in section 2.2, but implementing *SOC100_PVCurt* control strategy in the simulation process. We will consider that the inverters can modify their MPP fast and accurate enough to smooth upwards fluctuations, so the PV plant operates at full RRC during these events. However, for downwards fluctuations, a RRC assessment will be carried out for each k_p and k_c combination.

2.4 Complementary technique for fluctuations mitigation: Oversizing of PV array

The second technique proposed addresses PV+BESS plant configuration issues. As common practice, a good design criteria for properly matching inverters and PV array nominal powers is to keep the inverter-to-array ratio, named as DR_{INV}, between values of $0.7 < DR_{\mathrm{INV}} < 1.5$ (Lorenzo, 2014). However, given current PV module prices, oversizing the PV array with respect to the inverter output power range is a practice that is becoming popular. This way, DC PV power increases for an identical solar irradiance and, despite the inverters frequently operate in saturation, more total energy and in a less variable way is generated for the same nameplate power capacity, overcoming losses of DC side of the plant.

Moreover, due to current high battery investment costs, it could be profitable to oversize PV array if the fluctuations were reduced and as a consequence a battery with lower power and energy capacity requirements was needed to comply with RR_{LIM}. In other words, it could be more desirable to increment PV array size rather than battery size. An oversized PV array mitigates part of the fluctuations in the following two ways:

- When the area of the PV array is larger, high frequency fluctuations are mitigated by a low-pass filter smoothing effect (Hoff and Perez, 2010; Lave et al., 2012; Marcos et al., 2011a, 2011b).

- When PV array power $P_{\mathrm{PV,DC}}(t)$ is close to its peak power $P_{\mathrm{PV,p}}$, the inverter will saturate as DC power exceeds its rated capacity. When a cloud partially covers the array, a DC power fluctuation occurs, but at inverter level the fluctuation will only start when $P_{\mathrm{PV,DC}}(t)$ falls below its maximum input power. In other words, the fluctuation will be curtailed.

Hence, this technique is going to be studied in order to quantify its potential for the reduction of battery requirements, combining it with *SOC100_PVCurt* strategy.

2.4.1 Emulation of an oversized PV plant by means of artificial data series

The deep study of the PV array oversizing technique requires accurate output power data of an oversized plant, which will allow us to compare the latter with the original configuration of Milagro PV plant. The data series must include not only the effect of an oversizing parameter which scales-up the peak power of the PV array, but also the low pass filter effect due to its larger area. In order to include this phenomenon, two different artificial and comparable PV plants are going to be emulated. Both plants have a nameplate power capacity of $P_{\mathrm{N}} = 7.2$ MW but one of them has its PV array oversized by a factor $k_{\mathrm{os}} = 1.5$ respect to the other. Emulation of the original Milagro PV plant will be named as *Plant A* and it keeps the configuration of the real plant, being its inverter-to-array power ratio $DR_{\mathrm{INV}} = 0.8$. Emulation of the oversized Milagro PV plant will be named as *Plant B* and the inverter-to-array power ratio resulting from the oversizing process is $DR_{\mathrm{INV}} = 0.53$. Figure 3 describes the emulation of both plants.

The comparison must be as fair as possible and because of that, both data sources must be originated in the same way. As we do not have available measured data series of an oversized PV plant, both *Plant A* and *Plant B* power series are going to be created artificially by means of the technique developed in (Marcos et al., 2011b). This model creates the output power of a PV plant using as input the signal of the irradiance measured on the PV generator plane. It filters out high frequency components of the irradiance as a low-pass filter does, where the cut-off frequency depends on the surface area of the PV array.

For emulating *Plant A*, starting from an irradiance data series measured on-site in Milagro PV plant, the power data series of the plant is built. This data series is obtained as the output of the model, being *S* the real area of 52 ha and considering a *K* gain of 0.91 due to the degradation of the plant. For *Plant B*, we will consider a PV array area of S'=78 ha, which results from incrementing the original area proportionally by the oversizing factor k_{os}, while a *K* gain value of 0.91 is also used. Figure 4 describes the construction of the artificial power data series of both plants by means of the low-pass filter model technique.

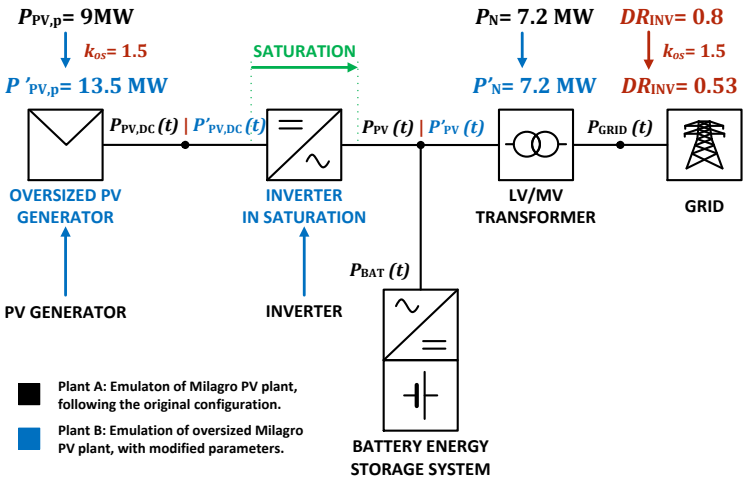

Figure 3: Emulation of two PV plants with artificial PV power data series. *Plant A* emulates original configuration of Milagro PV plant. *Plant B* emulates the oversizing of PV array by a factor of $k_{os} = 1.5$ and its inverter operates in saturation. Both plants have the same nameplate power $P_N = P'_N = 7.2$ MW.

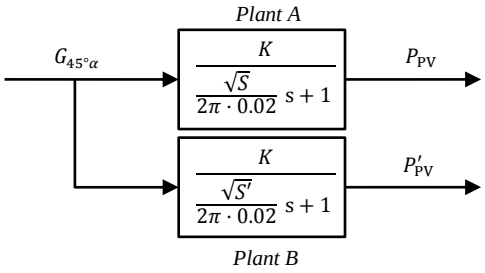

Figure 4: Low-pass filter transfer functions of *Plant A* and *Plant B*. The irradiance signal input is smoothed according to the cut-off frequency of each modelled plant, dependent of the square root of each area, obtaining as output the respective power signal.

Figure 5a shows, for a strong fluctuation, the input and output parameters of the previous model in the domain of time; normalised value of the irradiance incident on the inclined plane $G_{45°,\alpha}(t)$, and normalised output PV power of *Plant A* and *Plant B*, $P_{PV}(t)$ and $P'_{PV}(t)$ respectively. It can be seen that both PV plants act as low-pass filters of the irradiance signal, being stronger the filtering effect of the larger PV array. Figure 5b shows the absolute values for a whole day and Figure 5c is a zoomed detail of b. It can be seen that by saturating the inverters of *Plant B*, a good part of small fluctuations are curtailed.

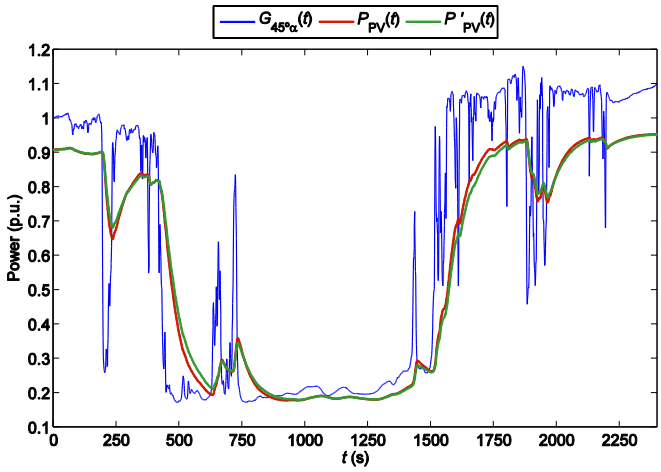

(a)

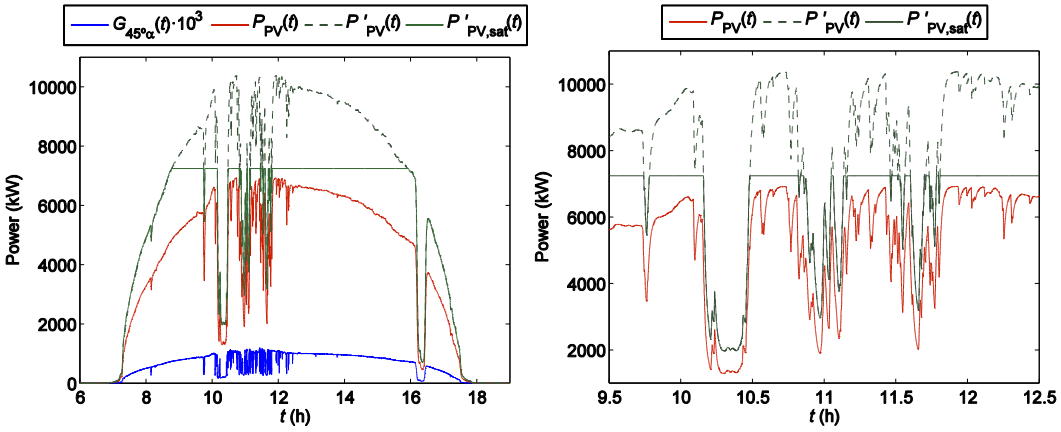

(b) (c)

Figure 5: Incident irradiance at inclined plane $G(45°, \alpha)$ at Milagro PV plant location and output PV power of *Plant A* and *Plant B* w/wo inverter saturation; normalised values in a time lapse of a fluctuation (a) and absolute values in a day, including zoomed lapse (b-c). The smoothing effect of the oversized PV array is observed in $P'_{PV}(t)$ power curve. Including the inverters saturation of *Plant B*, part of DC side fluctuations is curtailed (c).

2.4.2 *Battery size in an oversized PV plant: The Oversized Worst Fluctuation model*

When a PV array is oversized with respect to its inverters nameplate power, the instant output power $P'_{PV}(t)$ is limited to that value, but the fluctuations follow a shape characterised by the new PV array power $P'_{PV,DC}(t)$. For example, a downwards $P'_{PV,DC}(t)$ power fluctuation curve at the array following the WF model, is translated to a downwards $P'_{PV}(t)$ output power fluctuation curve starting at the saturation limit but following the shape of the first curve. Therefore, in order to size correctly the battery for absorbing every possible fluctuation, an *Oversized Worst Fluctuation* model is proposed, which takes into account the saturation point. In our emulation, this point is the nameplate power P'_N and its ratio respect to the maximum DC power $P'_{PV,DC,MAX}$ observed at the output of the oversized array is k_{os}^{-1}. Figure 6 shows the classic model and the update for implementing it in an oversized PV plant.

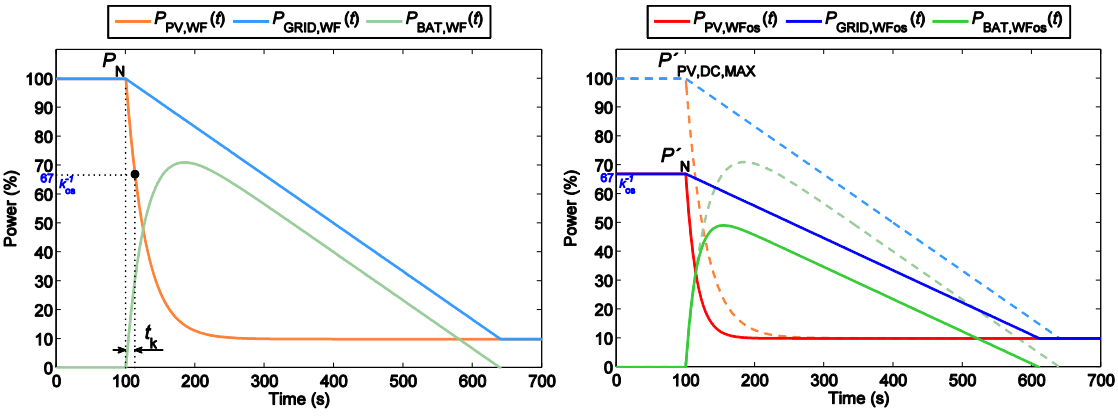

(a) (b)

Figure 6: (a) Worst Fluctuation model, defined in (Marcos et al., 2014b), where a downwards fluctuation at the array is outputted. (b) Oversized Worst Fluctuation model, where the fluctuation starts at the saturation point P'_N.

In the classic model defined in (Marcos et al., 2014b) and shown in Figure 6a, the worst PV power fluctuation is modelled as an exponential decay function, $P_{PV,WF}(t)$. The initial value or amplitude of the decay is set to $A = 90$ and the offset to $y_0 = 10$, modelling the transition from operating at 100% of P_N under clear sky conditions to 10% of P_N under diffuse irradiance, effect of the cloud coverage. r_{max} is the maximum slope of the power ramp allowed to inject to the grid $P_{GRID,WF}(t)$, in (%/s). But in the oversized case, the amplitude of $P_{PV,WF}(t)$ and the initial value and the slope of $P_{GRID,WF}(t)$ imposed in a

non-oversized plant, are adjusted to obtain the new power fluctuation curve $P_{\mathrm{PV,WFos}}(t)$ and the new output ramp $P_{\mathrm{GRID,WFos}}(t)$. The updated model takes into account that from the inverter point of view, the fluctuation starts at $P'_{\mathrm{N}} = k_{\mathrm{os}}^{-1} \cdot P'_{\mathrm{PV,DC,MAX}}$, being $k_{\mathrm{os}}^{-1} = 0.67$ in our case. Therefore, the new parameters are $A' = (100 \cdot k_{\mathrm{os}}^{-1}) - 10$ and $r'_{max} = k_{\mathrm{os}}^{-1} \cdot r_{\mathrm{max}}$.

Besides, a typical exponential decay function has a fast decaying behaviour during the first instants. After a certain time span set by the time constant defined as τ, it falls slower. In WF model, this value depends on the shortest dimension of the PV plant, *l*, in the following way.

$$\tau = 0.042 \cdot l - 0.5 \tag{2}$$

If we kept the original time constant as design criteria for the saturated fluctuation, we would disregard the fast decaying property of the beginning. In fast fluctuations which are not as strong as the worst case but that they occur during periods where the array is producing below P'_{N}, the fast decay will also reach inverter output level, so a battery sized for a slower decay would not be able to absorb it. Therefore, the *Oversized WF* model has a different time constant which is set as a reduction of the original τ (calculated using the *l* of the oversized array) by the time that the non-saturated curve lasts arriving from full-power to k_{os}^{-1}, named as t_k and defined in Figure 6a. The time constant is defined in the following Eq. (3).

$$\tau' = \tau - t_k \tag{3}$$

In this case, this means that t_k is the time span between 100% $P'_{\mathrm{PV,DC,MAX}}$ to 67% $P'_{\mathrm{PV,DC,MAX}}$ and it has a value of $t_k = 16.9$ s. We can define the *Oversized WF* model applying the adjustments to the original model, as defined in the following equations:

$$P_{\mathrm{PV,WFos}}(t) = A' \, e^{\left(-\frac{t}{\tau'}\right)} + 10 \tag{4}$$

$$P_{\mathrm{GRID,WFos}}(t) = A' - r'_{max} \, t + 10 \tag{5}$$

$$P_{\mathrm{BAT,WFos}}(t) = P_{\mathrm{PV,WF}}(t) - P_{\mathrm{GRID,WF}}(t) \tag{6}$$

where the instant values are calculated multiplying the nameplate capacity P_{N} and oversizing factor k_{os} by the Eqs. (4) - (6). The battery power for absorbing the fluctuation is given by $P_{\mathrm{BAT,WFos}}(t)$ and the instant value of this function along the fluctuation is given by Eq. (7).

$$P_{\mathrm{BAT,WFos}}(t) = \frac{k_{\mathrm{os}} \cdot P_{\mathrm{N}}}{100}\left[A'\left(1 - e^{-t/\tau'}\right) - r'_{max} \, t\right] \tag{7}$$

Obtaining the maximum of that function, the maximum battery power requirement is calculated:

$$P_{\mathrm{BAT,WFos}} = \frac{k_{\mathrm{os}} \cdot P_{\mathrm{N}}}{100}\left[A' - \tau' r'_{max}\left(1 + \ln\left|\frac{A'}{\tau' r'_{max}}\right|\right)\right] \tag{8}$$

where $P_{\mathrm{BAT,WFos}}$ is defined in (kW), r'_{max} in (%/s) and τ' in (s). In order to calculate the required energy capacity to face the fluctuation, Eq. (7) must be integrated along the time span that lasts from the beginning of the oversized worst fluctuation to the instant when the ramp reaches $0.1P'_{\mathrm{PV,DC,MAX}}$, defined as $T'_{\mathrm{R}} = A'/r'_{max}$.

$$C_{\mathrm{BAT,WFos}} = \int_0^{T'_{\mathrm{R}}} P_{\mathrm{BAT,WFos}}(t) \; dt = \frac{A' \cdot \; k_{\mathrm{os}} \cdot P_{\mathrm{N}}}{100 \cdot 3600}\left[\frac{A'}{2 \cdot r'_{max}} - \tau'\right] \tag{9}$$

where $C_{\mathrm{BAT,WFos}}$ is given in (kWh). In oversized PV plants, the battery requirements for absorbing 100% of the fluctuations will be the values given by the *Oversized WF* model, $P_{\mathrm{BAT,WFos}}$ and $C_{\mathrm{BAT,WFos}}$.

3. Results

3.1 Reduced size battery in combination with PV inverters limitation

Here the approach will be to compare *SOC100_PVCurt* strategy with *SOC50* strategy. First, the energy losses associated to inverters curtailment are quantified in order to delimit the negative impact of the new strategy, and second, its contributions to the battery size reduction potential are measured.

3.1.1 Energy losses caused by PV inverters limitation

Table 1 shows the PV production loss caused by inverters curtailments along a full year operation of the plant, in absolute terms and in function of the total available yearly PV energy. Six RR_{LIM} scenarios are considered to show its influence on the loss. For the RR_{LIM} = 10%/min scenario of our case, the loss is a negligible 0.57% and, for less restrictive limitations, it is even lower.

The RR_{LIM} of 2 %P_{N}/min is a strict requirement proposed in (CRE, 2012) and it serves us as scenario to evaluate the effectiveness of *SOC100_PVCurt*, by comparing its losses with those of the state of the art strategies studied in (de la Parra et al., 2016). In the cited study, it is stated that with a basic strategy the loss is more than 9%, while an advanced strategy reduces it to 2.33%. In the case of *SOC100_PVCurt*, it has an intermediate loss of 3.27%, so, given its simplicity, it is a good result.

Table 1: Annual energy loss associated with inverters limitation in upwards fluctuations, for different RR_{LIM} and operating a full-size battery under *SOC100_PVCurt* strategy.

RR_{LIM} in %P_{N}/min	$E_{\mathrm{PVi,Cu}}$ in MWh	$E_{\mathrm{PVi,Cu}}/E_{\mathrm{PV}}$ in %
2	509.2	3.27
5	214.2	1.37
7.5	131.3	0.84
10	89.1	0.57
20	27.9	0.18
30	11.2	0.07

3.1.2 Battery size reduction potential compared to SOC50 strategy

In order to evaluate the behaviour of reduced batteries operated by *SOC100_PVCurt* strategy against the *SOC50* strategy, the same simulations carried out in section 3.2 of (Makibar et al., 2017) have been carried out in a comparative way.

As a first comparison, the scenario where battery power P_{BAT} is reduced to 10% of $P_{\mathrm{BAT,WF}}$ is going to be analysed ($k_p = 0.1$, $k_c = 1$). Figure 7 shows in the same graphs the weekly evolution of four parameters, in blue if the PV plant is operated under *SOC100_PVCurt* strategy and in red if it is operated under *SOC50* strategy.

Figure 7a and b show respectively the RRC and the associated PV power curtailment factor along the year. Derived from them, Figure 7c and d show the weekly energy production and its loss due to penalties, with respect to maximum energy production of the PV plant obtained with full-power battery. It must be pointed out that, owing to the energy losses associated with inverters power limitation, the maximum production achievable with *SOC100_PVCurt* is slightly lower than the maximum production achievable with *SOC50*. However, the response of *SOC100_PVCurt* against battery size reduction is much better. For $k_p = 0.1$, *SOC100_PVCurt* achieves a better RRC along the year, falling into less curtailment penalties, which increases the PV energy production with respect to *SOC50*.

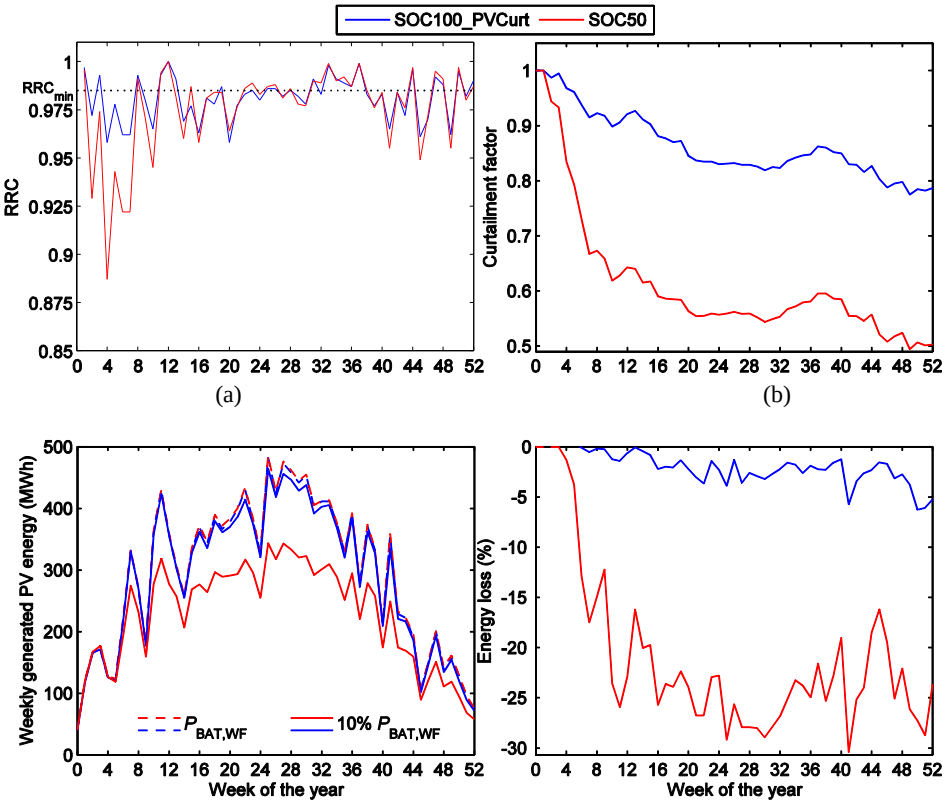

Figure 7: Yearly simulation of the PV plant operated by *SOC100_PVCurt* strategy, with a reduced battery ($k_p = 0.1$, $k_c = 1$) and comparing with the results of *SOC50* strategy. Weekly ramp rate compliance oscillates around $RRC_{\min}$ (a), generating fewer curtailments than *SOC50* along the year (b). Weekly energy loss with respect to full-power battery is low and total production is closer to the maximum achievable value (c and d).

Figure 8 and Figure 9 extend the simulation exercise to different power and capacity battery sizes. Figure 8 shows, for every k_p and k_c combination, the annual PV energy loss with respect to the one obtained with full-size battery. For every combination, the loss under *SOC100_PVCurt* is lower. It is limited to around 34% of the maximum generation in the no battery case, which is the scenario where only upwards fluctuations are absorbed by PV inverters curtailment. Moreover, there is no energy loss beyond 15% $P_{\mathrm{BAT,WF}}$ - 10% $C_{\mathrm{BAT,WF}}$ combination, placed in the corner of Figure 8a. This reduction limit is also lower than in *SOC50* case (30% $P_{\mathrm{BAT,WF}}$ - 15% $C_{\mathrm{BAT,WF}}$).

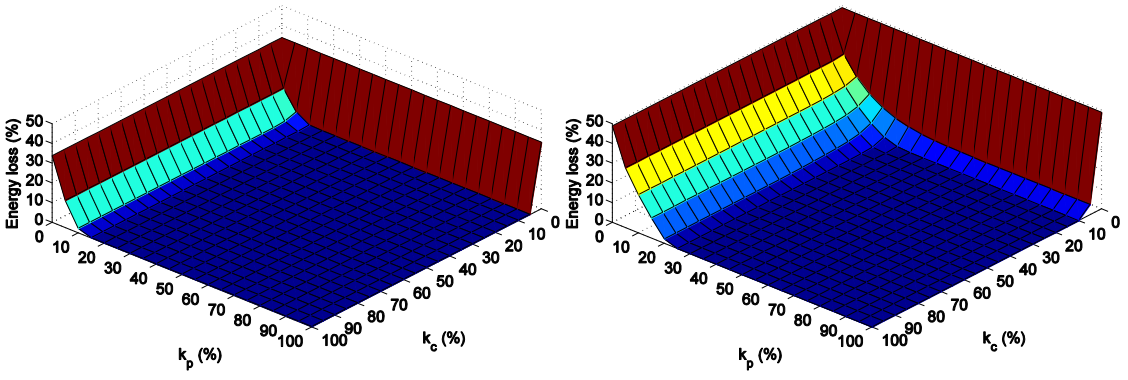

Figure 8: Annual energy loss with respect to full-size battery case, in function of power and capacity reduction factors k_p and k_c, implementing *SOC100_PVCurt* (a) vs. *SOC50* (b) control strategies.

Figure 9 shows the combinations of reduction of power and capacity of the battery that leads to a set of yearly PV plant production limits: 100%, 97%, 95% and 80% of the maximum achievable production. The 100% curve expresses the limit of the region containing possible k_p and k_c combinations that lead to 100% PV production, i.e., the set of combinations that minimise the size of the battery and avoid penalties operating always above RRC_{min}=98.5%. The maximum production obtained under *SOC100_PVCurt* strategy equals the production of the same plant operated under *SOC50* strategy but subtracting the energy loss associated with inverters power limitations. In this case, the loss is 0.57% (Table 1), so the 100% production limit of *SOC100_PVCurt* equals the 99.43% of the production of *SOC50*. Analogously, the 97% production limit of *SOC100_PVCurt* is equivalent to the 96.45% of the production of *SOC50*.

Some lines that keep the C-rate (P_{BAT}/C_{BAT} ratio) of batteries available in the market (Saft, 2016; Samsung SDI, 2016) have been added too, representing proportional reduction guides of their power and capacity. The intersections of production lines with these C-rate lines, give information about the annual produced energy using reduced batteries. The full-size battery is rated 11.8C ($P_{BAT,WF}$ / $C_{BAT,WF}$) and the corresponding reference C-rate line is drawn in dash-dot. As the design capacity under *SOC100_PVCurt* is the half of under *SOC50*, the reference C-rate is doubled (11.8C vs 5.9C).

The main difference of *SOC100_PVCurt* is that the 100% production region is larger, allowing a deeper battery size reduction. Besides, as the new reference C-rate is higher, the commercial battery C-rate lines used here will lie below the reference dash-dot line of 11.8C. That means that *SOC100_PVCurt* strategy requires a battery with higher power than *SOC50*, being less determinant the energy capacity. This fact becomes evident by checking that production limit lines are more separated along k_p axis than along k_c axis. In other words, the reduction of battery power has more effect in PV production loss than the reduction of battery capacity.

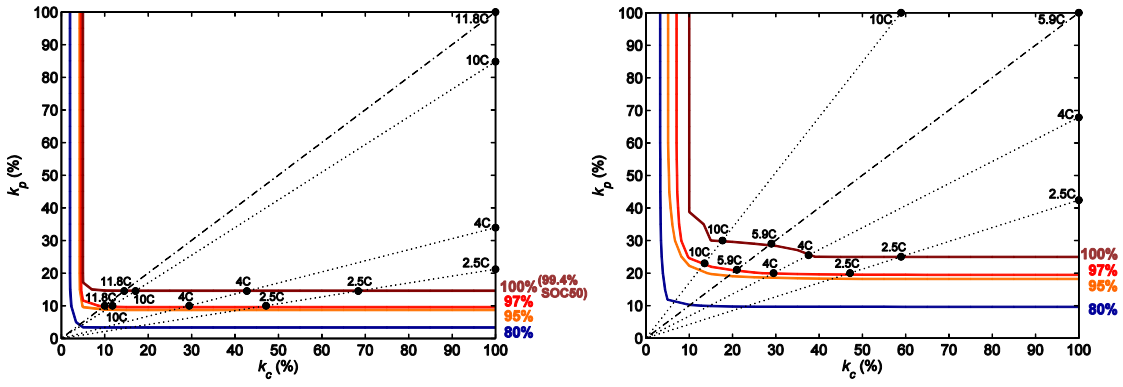

Figure 9: Different annual production percentage limits with respect to maximum achievable one, depending on k_p and k_c combinations and implementing *SOC100_PVCurt* (a) vs. *SOC50* (b). Dotted lines represent k_p and k_c combinations that keep C-rates of commercial batteries, being them in reference to WF model battery C-rate (11.8C vs. 5.9C) in dash-dot line.

Table 2 describes as an example some significant points of Figure 9a, corresponding with reductions of four batteries to keep 100% and 97% annual PV generation targets. For comparison purposes, the points with equivalent energy production limits obtained with *SOC50* simulations are included.

Main conclusion is that with *SOC100_PVCurt*, both battery power and capacity requirements are 40-50% lower. It must be noted that in the case of reference C-rate, the especially high save in capacity is due to changing from 5.9C to 11.8C. Besides, with *SOC100_PVCurt*, the required battery power to achieve each PV production limit is constant for every C-rate, so, the lower the C-rate of the commercial battery used is, the higher the capacity requirement will be. This fact can be seen as a battery technology limitation.

Table 2: Battery size vs. PV energy production for different commercial C-rates, comparing results between *SOC100_PVCurt* and *SOC50* strategies.

E_{GRID} limit	C-rate	*SOC100_PVCurt*		*SOC50*		Saving	
		Power in kW (*% of* P_N)	Capacity in kWh (*min*)	Power in kW (*% of* P_N)	Capacity in kWh (*min*)	Power (%)	Capacity (%)
100%	11.8/5.9	747 (*10.3*)	64 (*0.5*)	1261 (*17.4*)	214 (*1.8*)	41	70
(99.43%	10	747 (*10.3*)	75 (*0.6*)	1313 (*18.1*)	132 (*1.1*)	43	43
SOC50)	4	747 (*10.3*)	187 (*1.6*)	1236 (*17.1*)	309 (*2.6*)	40	39
	2.5	747 (*10.3*)	299 (*2.5*)	1236 (*17.1*)	495 (*4.1*)	40	40
97%	11.8/5.9	515 (*7.1*)	44 (*0.4*)	1030 (*14.2*)	175 (*1.5*)	50	75
(96.45%	10	515 (*7.1*)	52 (*0.4*)	1159 (*16.0*)	116 (*1.0*)	56	55
SOC50)	4	515 (*7.1*)	129 (*1.1*)	1004 (*13.9*)	251 (*2.1*)	49	49
	2.5	515 (*7.1*)	206 (*1.7*)	1004 (*13.9*)	402 (*3.3*)	49	49

3.2 Oversized PV array and inverters operation in saturation

3.2.1 Battery size reduction in an oversized PV plant

In order to analyse the behaviour of reduced batteries operated by *SOC100_PVCurt* strategy in an oversized PV plant, with the emulated plants as scenarios, two parallel extensive simulation rounds of battery size reduction assessment are carried out for every k_p and k_c combination. The simulation round corresponding to *Plant A* uses the artificial series of $P_{\mathrm{PV}}(t)$ as input and the battery considered as starting point is sized according to the classic WF model: $P_{\mathrm{BAT,WF}} = 5148\,\mathrm{kW}$ and $C_{\mathrm{BAT,WF,os}} = 437\,\mathrm{kWh}$ (11.8C). The simulation round corresponding to *Plant B* uses the series of $P'_{\mathrm{PV}}(t)$ and the battery is sized according to the Oversized WF model: $P_{\mathrm{BAT,WFos}} = 5182\,\mathrm{kW}$ and $C_{\mathrm{BAT,WFos}} = 408\,\mathrm{kWh}$ (12.7C). Figure 10 shows the annual energy loss of each plant with respect to the production with full-size battery.

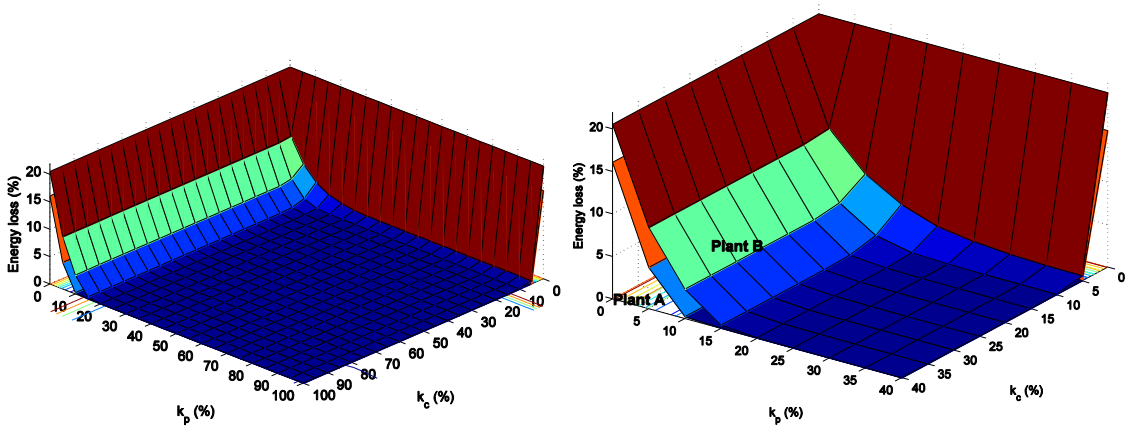

(a) (b)

Figure 10: Annual energy loss with respect to full-size battery case, in function of k_p and k_c, comparing *Plant A* (7.2 MW) and *Plant B* (7.2 MW / PV array oversized); (b) is a detail of the corner section of (a). An oversized PV plant has more losses for the same battery reduction rate than a non-oversized plant.

Figure 10b is a zoom detail of the corner area of Figure 10a. It can be seen that the energy loss of the oversized *Plant B* starts to increase with higher battery requirements than in *Plant A*; especially in power, 5% higher. This fact means that the ramp rate failures are higher when reducing a battery in an oversized plant than in a non-oversized plant. Moreover, in the no battery case there are more losses, which means that *Plant B* falls into more total penalties.

Figure 11a and Figure 11b show the production limits & C-rates graph for *Plant A* and *Plant B* respectively, where each reference C-rate corresponds to the design battery size of each plant.

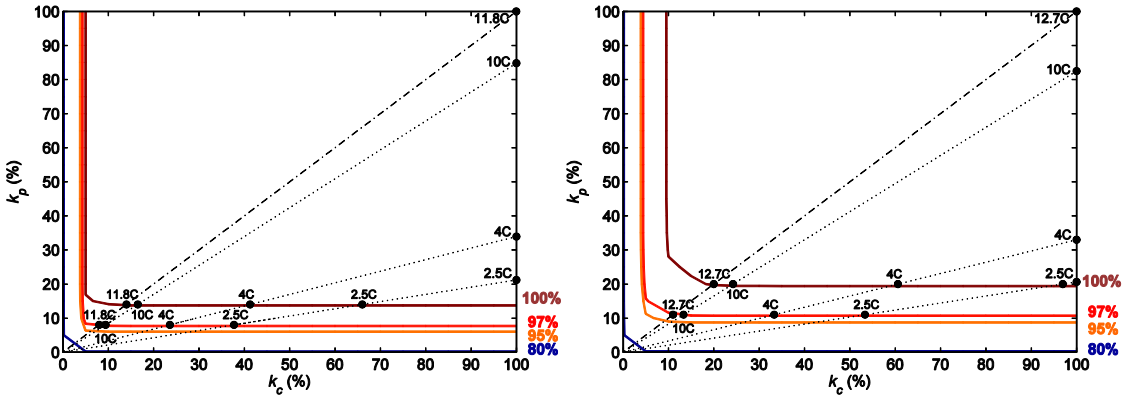

(a) (b)

Figure 11: Different annual production percentage limits with respect to maximum achievable one, depending on k_p and k_c combinations for non-oversized *Plant A* (a) and oversized *Plant B* (b). Penalties caused by battery reduction affect more to an oversized PV plant, having less battery size reduction potential.

In both cases, production limits are more separated along k_p axis than along k_c axis, but the separation is higher in the oversized plant, reducing its 100% production region. Hence, *Plant B* is more sensitive to battery power and capacity reductions than *Plant A*, so some kind of power and energy demanding fluctuation events must affect more to the oversized plant than to the non-oversized one. In order to find out this phenomenon, an exhaustive analysis of the fluctuations events of an oversized plant is carried out in the next section.

3.2.2 Fluctuations events characterisation in an oversized PV plant

The deep study of downwards fluctuations events at an oversized PV plant is done by characterising battery power and energy responses to mitigate them. If we split into bins of histograms the battery power and energy series of the simulated year, we can define certain power or energy requirement intervals. These histograms are shown in Figure 12, for either *Plant A* and *Plant B*. The series are normalised and placed in between intervals of 10%, taking as reference the largest power or energy requirement to smooth the largest fluctuation of the year ($P_{\mathrm{BAT,MAX}}$ and $E_{\mathrm{BAT,MAX}}$).

Battery power discharge events are distributed as described in Figure 12a. As seen, low power fluctuations have less frequency in the oversized *Plant B* than in *Plant A*. This is consistent with the high frequency components attenuation effect provided by a larger PV array, but also with the low power fluctuations curtailment entailed by the saturation of the inverters.

However, in *Plant B* power demands around 0.2 - 0.5 of $P_{\mathrm{BAT,MAX}}$ are amplified with respect to *Plant A*. This amplification makes *Plant B* more sensitive to battery power reduction because when it is reduced, the amplified demands cannot be covered and RR_{LIM} failures occur. Figure 12b shows both the amplification of medium power events and the attenuation of low power events mentioned before.

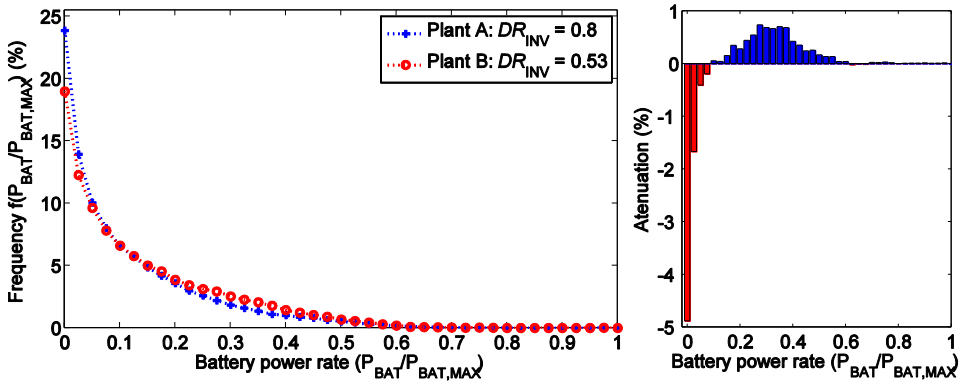

(a) (b)

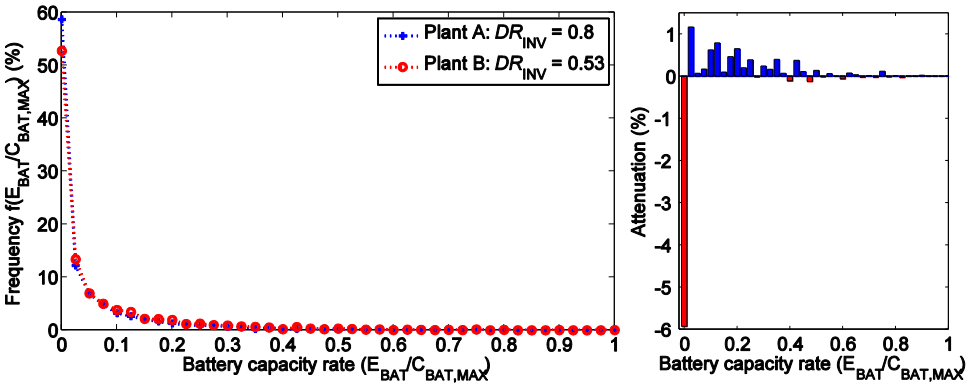

(c) (d)

Figure 12: Histograms of battery power (a) and energy (c) managed during downwards fluctuations; for *Plant A* and *Plant B*. In an oversized plant, low power and energy downwards fluctuations are smoothed by the oversizing technique, while medium size events are amplified (b and d).

In the case of battery discharge energy events shown in Figure 12c and d, the difference with respect to *Plant A* occurs mainly in very low energy demanding events.

Figure 13 illustrates the effects in the time domain, showing three hours of operation of *Plant A* and *Plant B* before midday of a highly fluctuating day. First, it is interesting to point out how the battery power signal of *Plant B* is attenuated filtering out the high frequency noise. Second, the amplification of two medium-size power events takes place at t_1 and at t_2. The first event requires a maximum battery power of $P_{\mathrm{BAT}}(t_1) = 2331$ kW in *Plant A* and it is amplified to $P'_{\mathrm{BAT}}(t_1) = 2853$ kW in *Plant B*. The second one is amplified from $P_{\mathrm{BAT}}(t_2) = 1367$ kW to $P'_{\mathrm{BAT}}(t_2) = 1767$ kW. As the array is oversized, the PV power fall of these events is amplified by the oversizing factor while the allowed RR_{LIM} is the same, so the required battery power is higher.

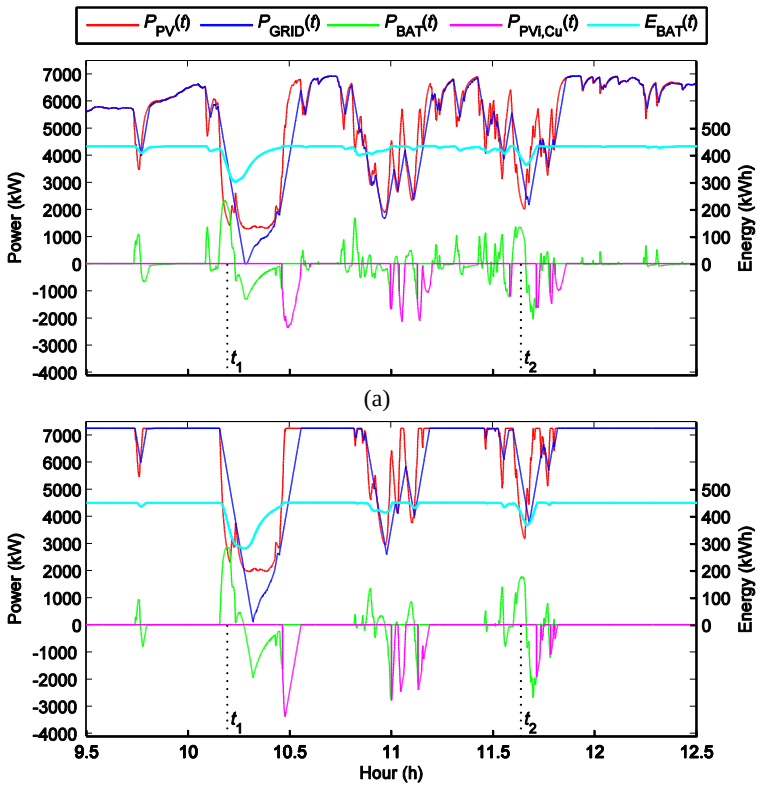

(a)

(b)

Figure 13: Battery and inverter limitations in operation around midday on a highly fluctuating day, in *Plant A* (a) and in oversized *Plant B* (b). High frequency components of battery power operation are smoothed by means of the oversizing technique. However, some medium-size components are amplified like discharges at t_1 and at t_2.

It is also worth mentioning a side effect of this behaviour. The filtering of low power and high frequency operation signal of the battery leads to reducing its yearly operating time by 10%. Regarding the cycling degradation caused by the time of use, it can be an important save.

3.2.3 Comparative study of the reduction techniques

In order to assess the battery size reduction potentials of the two novel techniques in a fair way, we are going to compare the yearly energy production (E_{GRID}) obtained in *Plant A* with the production obtained in *Plant B* if the same battery was installed. Besides, if we add to the comparison the energy that would produce *Plant A* operated by *SOC50*, we can compare all three techniques developed between (Makibar et al., 2017) and this paper, enumerated as follows: *Technique 1* is the size reduction of a battery operated under *SOC50* strategy, *Technique 2* implements *SOC100_PVCurt* strategy and *Technique 3* combines *SOC100_PVCurt* with PV array oversizing.

Three scenarios with three battery sizes are compared in Table 3, using a 10C configuration as a showcase. In first scenario, the battery size used as a reference is the most reduced one that allows *Plant A* to operate under *SOC100_ PVCurt* without falling into penalties, leading to maximum production. The power and capacity combination of that battery lies on the intersection between the 100% limit curve and the 10C line of Figure 11a, which is rated $P_{\mathrm{BAT,10C}}$ = 721 kW and $C_{\mathrm{BAT,10C}}$ = 72 kWh. The second and third scenarios use battery sizes that allow 95% and 90% of the maximum production respectively.

The exercise must be considered as sequential implementations of each technique and two approaches are used for the analysis: first, evaluating the PV production of each technique for a same battery size; second, evaluating the effect of reducing a battery from one scenario to the next while implementing each technique.

Table 3: PV energy production obtained in an emulation of the Milagro PV plant (7.2 MW) with three sizes of a 10C commercial battery and implementing the three techniques developed in this work: *Technique 1* (*Plant A* under SOC50), *Technique 2* (*Plant A* under SOC100_PVCurt) and *Technique 3* (oversized *Plant B* under SOC100_PVCurt). The reference battery size is the one that allows *Plant A* to achieve 100% of PV production without falling into penalties. %MAX E_{GRID} is the percentage of the maximum achievable production at each plant.

Scenario (Size red.)	P_{BAT} in kW (*% of* P_{N})	C_{BAT} in kWh (*min*)	Technique 1		Technique 2		Technique 3		ΔE_{GRID} 1→2 %	ΔE_{GRID} 2→3 %
			E_{GRID} in MWh	%MAX E_{GRID} A	E_{GRID} in MWh	%MAX E_{GRID} A	E_{GRID} in MWh	%MAX E_{GRID} B		
1	721 (*10.0*)	72 (*0.6*)	13 628	90.8%	14 930	100%	18 784	98.3%	9.6	25.8
2 (-53%)	335 (*4.6*)	34 (*0.3*)	11 407	76%	14 183	95%	17 427	91.2%	24.3	22.9
3 (-70%)	216 (*3.0*)	22 (*0.2*)	10 281	68.5%	13 437	90%	16 529	86.5%	30.7	23.0

Following the first approach, it can be seen that in all three scenarios, for the same battery, each new technique improves the PV production of the previous one. Comparing *Technique 1* and *Technique 2*, in spite of the losses associated with the inverters limitation, the latter has a higher battery size reduction potential; which allows for an increase in PV production.

Regarding the two novel solutions, *Technique 2* and *Technique 3*, *Plant B* produces more than *Plant A*; e.g., 25% more in scenario 1. It is interesting to see that, respect to its own production, the oversized plant falls into more penalties because it is more sensitive to the battery size reduction. While *Plant A* produces its 100% (no penalties), *Plant B* produces its 98.3% achievable energy (penalties cause a loss of 1.7%). However, it produces more energy. But this is achieved by oversizing the PV array by a factor of 1.5, which means that the number of PV modules is increased by 50%. In this sense, this table can be seen as a tool to evaluate if the 50% of increase in the investment costs of the PV array is compensated along the life of the project with the 25% of increase in the yearly PV production.

Following the second approach, it can be seen that, with each technique, the battery can be significantly reduced without losing production. Comparing the novel techniques, the battery can be reduced by a 70%, from a size of P_{BAT} = 721 kW and C_{BAT} = 72 kWh (scenario 1, *Plant A* produces 14.9 GWh under *Technique 2*) to a size of P_{BAT} = 216 kW and C_{BAT} = 22 kWh (scenario 3, *Plant B* produces 16.5 GWh under *Technique 3*) not only without losing PV production, but also increasing it by 10.7%. Therefore, project developers can use this tool to evaluate if, at the expense of increasing 50% the number of PV modules, the project could improve its feasibility by saving costs thanks to 70% less battery requirements and thanks to increasing yearly PV production by 10.7%.

For a full comparison of all three techniques, we can follow this process: Under *Technique 1*, the battery of scenario 1, rated P_{BAT} = 721 kW and C_{BAT} = 72 kWh, leads to a PV production of 13.6 GWh. If *SOC100_PVCurt* strategy is implemented (*Technique 2)* and the battery is reduced by 53% down to P_{BAT} = 335 kW and C_{BAT} = 34 kWh, PV production would even increase by 4% to 14.2 GWh. If then the oversizing technique is implemented (*Technique 3*) and the battery is reduced by an extra 35% down to P_{BAT} = 216 kW and C_{BAT} = 22 kWh, the production would increase by 16% to 16.5 GWh.

4. Conclusions and outlook

This work has presented two new techniques to contribute to reduce the storage requirements for PV power ramp rate control. In particular, they enhance a battery size reduction assessment method developed in a previous work which implemented a basic SOC control strategy.

The first technique is based on the fact that the battery size can be reduced if upwards fluctuations are mitigated by moving the operation of PV inverters out of their MPP. Hence, a novel control strategy named as *SOC100_PVCurt* has been developed, which fulfils the ramp rate control requirements combining effectively the operation of reduced batteries and PV inverters power limitation. By recovering the SOC of the battery during upwards fluctuations, less PV inverters limitations are necessary and the associated energy loss is considerably reduced. For *RR* = 10%/min, this strategy allows for reducing the power and capacity requirements an extra 40% - 50% with respect to the basic *SOC50* strategy, at the expense of a negligible PV production loss of 0.57% due to inverters power limitation.

The second technique has been developed for reducing the high-frequency and low power fluctuations of the PV plant by oversizing its PV array, and, consequently, for reducing storage requirements. The results show an interesting effect when applying the size reduction assessment to a plant with its PV array oversized by 1.5. Although the high frequency and low power fluctuations and the associated battery discharge power events are attenuated up to 5%, medium power events are amplified; which implies that, when the battery power is progressively reduced, the oversized plant falls into ramp rate failures with a lower reduction degree than a non-oversized one. However, comparing to the PV production of a non-oversized plant, with the oversizing technique the battery can be significantly reduced without losing production. For instance, a battery that allows a non-oversized plant reaching its maximum PV production without falling into penalties can be reduced by a 70% if the PV array is oversized, not only without losing PV production, but also increasing it by 10.7%. The study has presented tools to evaluate if, at the expense of oversizing the PV array, a project could improve its feasibility by saving battery costs and by increasing PV production.

These results are interesting for PV plant projects developers and for battery manufacturers. The combination of battery size reduction with inverters limitation and PV array oversizing arises multiple decision factors. The battery requirements in an oversized PV plant changes radically from the classic PV plants, so this study should be taken into account to find the optimal *battery size-PV array-inverter power* ratios.

5. References

Bullich-Massagué, E., Aragüés-Peñalba, M., Sumper, A., Boix-Aragones, O., 2017. Active power control in a hybrid PV-storage power plant for frequency support. Sol. Energy 144, 49–62. doi:10.1016/j.solener.2016.12.033

Chowdhury, B.H., 1992. Optimizing the integration of photovoltaic systems with electric utilities. IEEE Trans. Energy Convers. 7, 72–78. doi:10.1109/60.124544

Chowdhury, B.H., Rahman, S., 1987. Forecasting sub-hourly solar irradiance for prediction of photovoltaic output, in: IEEE Photovoltaic Specialists Conference, 19th, New Orleans, LA, May 4-8, 1987, Proceedings (A88-34226 13-44). New York, Institute of Electrical and Electronics Engineers, Inc. pp. 171–176.

CRE, 2012. Comisión Reguladora de Energía: Reglas generales de interconexión al sistema eléctrico nacional.

de la Parra, I., Marcos, J., García, M., Marroyo, L., 2016. Improvement of a control strategy for PV power ramp-rate limitation using the inverters : reduction of the associated energy losses. Sol. Energy.

de la Parra, I., Marcos, J., García, M., Marroyo, L., 2015. Control strategies to use the minimum energy storage requirement for PV power ramp-rate control. Sol. Energy 111, 332–343. doi:10.1016/j.solener.2014.10.038

EPIA, 2012. Connecting the sun. Solar photovoltaics on the road to large-scale grid integration.

HECO, 2014. Hawaiian Electric Company: State of the system, summary for ESS RFP.

Hoff, T.E., Perez, R., 2010. Quantifying PV power output variability. Sol. Energy 84, 1782–1793. doi:10.1016/j.solener.2010.07.003

Ina, N., Yanagawa, S., Kato, T., Suzuoki, Y., 2004. Smoothing of PV system output by tuning MPPT control. IEEJ Trans. Power Energy 124, 455–461.

Lave, M., Kleissl, J., 2013. Cloud speed impact on solar variability scaling - Application to the wavelet variability model. Sol. Energy 91, 11–21. doi:10.1016/j.solener.2013.01.023

Lave, M., Kleissl, J., Arias-Castro, E., 2012. High-frequency irradiance fluctuations and geographic smoothing. Sol. Energy 86, 2190–2199. doi:10.1016/j.solener.2011.06.031

Lorenzo, E., 2014. Electricidad Solar Fotovoltaica, VIII: Ingeniería Fotovoltaica. PROGENSA.

Makibar, A., Narvarte, L., Lorenzo, E., 2017. On the relation between battery size and PV power ramp rate limitation. Sol. Energy 142, 182–193. doi:10.1016/j.solener.2016.11.039

Marcos, J., de La Parra, I., García, M., Marroyo, L., 2014a. Control strategies to smooth short-term power fluctuations in large photovoltaic plants using battery storage systems. Energies 7, 6593–6619. doi:10.3390/en7106593

Marcos, J., Marroyo, L., Lorenzo, E., Alvira, D., Izco, E., 2011a. Power output fluctuations in large scale PV plants: One year observations with one second resolution and a derived analytic model. Prog. Photovoltaics Res. Appl. 19, 218–227. doi:10.1002/pip.1016

Marcos, J., Marroyo, L., Lorenzo, E., Alvira, D., Izco, E., 2011b. From irradiance to output power fluctuations: the PV plant as a low pass filter. Prog. Photovoltaics Res. Appl. 19, 505–510. doi:10.1002/pip.1063

Marcos, J., Marroyo, L., Lorenzo, E., García, M., 2012. Smoothing of PV power fluctuations by geographical dispersion. Prog. Photovoltaics Res. Appl. 20, 226–237. doi:10.1002/pip.1127

Marcos, J., Storkël, O., Marroyo, L., García, M., Lorenzo, E., 2014b. Storage requirements for PV power ramp-rate control. Sol. Energy 99, 28–35. doi:10.1016/j.solener.2013.10.037

Mazumdar, B.M., Saquib, M., Das, A.K., 2014. An empirical model for ramp analysis of utility-scale solar PV power. Sol. Energy 107, 44–49. doi:10.1016/j.solener.2014.05.027

Mills, A., Ahlstrom, M., Brower, M., Ellis, A., George, R., Hoff, T., Kroposki, B., Lenox, C., Miller, N., Stein, J., Wan, Y.H., 2009. Understanding variability and uncertainty of photovoltaics for integration with the electric power system. Lawrence Berkeley Natl. Lab.

Murata, A., Otani, K., 1997. An analysis of time-dependent spatial distribution of output power from very

654 many PV power systems installed on a nation-wide scale in Japan. Sol. Energy Mater. Sol. Cells 47,
655 197–202. doi:10.1016/S0927-0248(97)00040-8

656 Murata, A., Yamaguchi, H., Otani, K., 2009. A method of estimating the output fluctuation of many
657 photovoltaic power generation systems dispersed in a wide area. Electr. Eng. Japan (English Transl.
658 Denki Gakkai Ronbunshi) 166, 9–19. doi:10.1002/eej.20723

659 NERC, 2012. North American Electric Reliability Corporation: Interconnection requirements for variable
660 generation. Atlanta.

661 Otani, K., Minowa, J., Kurokawa, K., 1997. Study on areal solar irradiance for analyzing areally-totalized
662 PV systems. Sol. Energy Mater. Sol. Cells 47, 281–288. doi:10.1016/S0927-0248(97)00050-0

663 Perez, R., Hoff, T.E., 2013. Mitigating short-term PV output intermittency, in: 28th European
664 Photovoltaic Solar Energy Conference and Exhibition. pp. 3719–3726.

665 PREPA, 2012. Puerto Rico Electric Power Authority minimum technical requirements for photovoltaic
666 (PV) generation projects.

667 Saft, 2016. Energy storage systems market brochure - www.saftbatteries.com.

668 Samsung SDI, 2016. ESS for utility commercial - www.samsungsdi.com.

669 Sukumar, S., Mokhlis, H., Mekhilef, S., Karimi, M., Raza, S., 2018. Ramp-rate control approach based on
670 dynamic smoothing parameter to mitigate solar PV output fluctuations. Electr. Power Energy Syst.
671 96, 296–305. doi:10.1016/j.ijepes.2017.10.015

672 Tomson, T., Tamm, G., 2006. Short-term variability of solar radiation. Sol. Energy 80, 600–606.
673 doi:10.1016/j.solener.2005.03.009

674 van Haaren, R., Morjaria, M., Fthenakis, V., 2015. An energy storage algorithm for ramp rate control of
675 utility scale PV (photovoltaics) plants. Energy 91, 894–902. doi:10.1016/j.energy.2015.08.081

676 Van Haaren, R., Morjaria, M., Fthenakis, V., 2014. Empirical assessment of short-term variability from
677 utility-scale solar PV plants. Prog. Photovoltaics Res. Appl. 22, 548–559. doi:10.1002/pip.2302

678 Woyte, A., Belmans, R., Nijs, J., 2007a. Localized spectral analysis of fluctuating power generation from
679 solar energy systems. EURASIP J. Adv. Signal Process. 2007. doi:10.1155/2007/80919

680 Woyte, A., Belmans, R., Nijs, J., 2007b. Fluctuations in instantaneous clearness index: Analysis and
681 statistics. Sol. Energy 81, 195–206. doi:10.1016/j.solener.2006.03.001

682 Woyte, A., Thong, V. Van, Belmans, R., Nijs, J., 2006. Voltage fluctuations on distribution level
683 introduced by photovoltaic systems. IEEE Trans. Energy Convers. 21, 202–209.
684 doi:10.1109/TEC.2005.845454

685